Microwave-Assisted Synthesis of a Core–Shell MWCNT/GONR Heterostructure for the Electrochemical Detection of Ascorbic Acid, Dopamine, and Uric Acid

Chia-Liang Sun,[†,*] Ching-Tang Chang,[†] Hsin-Hsien Lee,[†] Jigang Zhou,[‡] Jian Wang,[‡] Tsun-Kong Sham,[§] and Way-Faung Pong[⊥]

[†]Department of Chemical and Materials Engineering, Chang Gung University, Kwei-Shan, Tao-Yuan 333, Taiwan, [‡]Canadian Light Source Inc., University of Saskatchewan, Saskatoon, Canada S7N 0X4, [§]Department of Chemistry, University of Western Ontario, London, Canada N6A 5B7, and [⊥]Department of Physics, Tamkang University, Tamsui 251, Taiwan

ABSTRACT In this study, graphene oxide nanoribbons (GONRs) were synthesized from the facile unzipping of multiwalled carbon nanotubes (MWCNTs) with the help of microwave energy. A core–shell MWCNT/GONR-modified glassy carbon (MWCNT/GONR/GC) electrode was used to electrochemically detect ascorbic acid (AA), dopamine (DA), and uric acid (UA). In cyclic voltammograms, the MWCNT/GONR/GC electrode was found to outperform the MWCNT- and graphene-modified GC electrodes in terms of peak current. For the simultaneous sensing of three analytes, well-separated voltammetric peaks were obtained using a MWCNT/GONR/GC electrode in differential pulse voltammetry measurements. The corresponding peak separations were 229.9 mV (AA to DA), 126.7 mV (DA to UA), and 356.6 mV (AA to UA). This excellent electrochemical performance can be attributed to the unique electronic structure of MWCNTs/GONRs: a high density of unoccupied electronic states above the Fermi level and enriched oxygen-based functionality at the edge of the graphene-like structures, as revealed by X-ray absorption near-edge structure spectroscopy, obtained using scanning transmission X-ray microscopy.

KEYWORDS: graphene oxide nanoribbon · multiwalled carbon nanotube · microwave · electrochemical biosensor · ascorbic acid · dopamine · uric acid

Carbon is one of the most abundant elements in nature, and novel nanoscale carbon crystalline forms have been predicted and synthesized over the past few decades. In 1985, C_{60} (buckminsterfullerene) was discovered when graphite was vaporized by laser irradiation.[1] In 1991, Iijima reported the transmission electron microscopy (TEM) analysis of carbon nanotubes (CNTs) prepared by the arc-discharge evaporation method, and studies of CNTs have subsequently attracted great attention.[2−9] In 2004, Novoselov *et al.* first isolated individual graphene planes using Scotch tape and found that graphene has great potential for applications in electronics.[10−13] Additionally, Nakada *et al.* predicted the existence of graphene nanoribbons (GNRs) theoretically in 1996.[14] Until recently, graphene nanoribbons have been fabricated by scanning tunneling microscope lithography and chemical vapor deposition.[15,16] The effect of the structure on the band gaps of GNRs has been widely investigated.[17,18] In addition to the above-mentioned methods, CNTs have been more recently utilized as the starting material to obtain GNRs.[19,20] In the literature, the process to create GNRs from CNTs can be divided into several categories, including wet chemical methods,[21−23] physicochemical methods,[24] intercalation–exfoliation,[25] catalytic approaches,[26,27] electrical methods,[28] sonochemical methods,[29] and electrochemical methods.[30] However, opportunities still exist to use a facile and large-scale unzipping process. In many of the published examples, microwave heating has been shown to dramatically reduce reaction time, increase product yields, and enhance product purities by reducing unwanted side reactions compared with conventional heating methods.[31] More recently, the advantages of this enabling technology have also been exploited.[32−36] Carbon materials with dipolar polarization and conduction are excellent microwave absorbers.[37−40] The purification and functionalization of CNTs can be accomplished through a microwave treatment.[41−44] Zhu *et al.* synthesized activated microwave-exfoliated graphite oxide (a-MEGO) with a Brunauer–Emmett–Teller surface area of up to 3100 m^2/g as well as excellent gravimetric capacitance and energy density.[36] Therefore, it is of interest to investigate the effects of

* Address correspondence to sunchialiang@gmail.com.

Received for review May 1, 2011 and accepted September 12, 2011.

Published online September 12, 2011
10.1021/nn2015908

microwave energy on the unzipping process when CNTs are used as the raw material.

Dopamine (DA) has been demonstrated to be a neurotransmitter in the brain; hence, it sheds light on the treatment of disorders of the central nervous system, such as Parkinson's disease.[45,46] Since the 1970s, electrochemical methods have been used to detect chemicals in the brain.[47−49] Because the electrochemical oxidation peak potentials for ascorbic acid (AA), DA, and uric acid (UA) are similar, research has focused on how to separate their signal potentials with enhanced intensity.[50−54] CNTs have been widely utilized in the electrochemical detection of biomolecules, although there is still uncertainty about the fundamental activity of CNTs as electrode materials.[55−58] More specifically, CNTs have been applied to the electrochemical sensing of AA, DA, and UA because of their unique electronic structures and conductivites.[59−63] Recently, platelet graphite nanofibers were found to exhibit faster heterogeneous electron transfer rates than MWCNTs and graphite microparticles for a wide variety of compounds because of their graphene sheet orientation.[64] Graphene-based nanomaterials have also attracted attention for electrochemistry applications, including energy storage and sensing.[65−67] Shang *et al.* reported a novel microwave plasma-enhanced chemical vapor deposition strategy to grow multilayer graphene films for biosensing.[68] Zhou *et al.* proposed a chemically reduced graphene-oxide-modified glassy carbon electrode as an electrochemical sensing and biosensing platform.[69] Wang *et al.* applied a graphene-modified electrode for the selective detection of DA.[70] Lim *et al.* found that anodized epitaxial graphene is a superior electroanalytical platform for a wide range of biomolecules.[71] Kim *et al.* synthesized a graphene-modified electrode for the selective detection of DA.[72] Sun *et al.* reported that a Pt−graphene composite has a better oxidation current for AA, DA, and UA than graphene in electrochemical measurements.[73] Except for the enhanced electrochemical Li storage of GNRs,[74,75] there has been little research performed on the electrochemistry of GNRs. Herein, we present the simultaneous electrochemical detection of three analytes using graphene oxide nanoribbons (GONRs) fabricated by the microwave-assisted facile unzipping of MWCNTs. To gain insight into the intrinsic relationship between the electronic structure and performance of this novel core/shell structure, we performed spectromicroscopic studies using scanning transmission X-ray microscopy, which has been widely validated in the study of single nanostructures. Indeed, the electronic structure of a single MWCNT/GONR core/shell was elucidated by C K-edge X-ray absorption near-edge structure spectroscopy.

RESULTS AND DISCUSSION

Figure 1 shows transmission electron microscopy (TEM) images of the power-dependent morphological evolution of the tube-to-ribbon transformation. The stepwise opening of MWCNTs to form nanoribbons is depicted after treatment under different microwave powers from 150 to 250 W at a constant time of 4 min. During the reaction at the lowest microwave power (150 W), as shown in Figure 1b, the unzipping started at one side wall of the nanotube to form a thinner graphene wing than that of the as-received nanotube shown in Figure 1a. For the reaction at 200 W, Figure 1c illustrates that graphene sheet structures were found on both sides of the nanotubes, whereas the central cores of nanotubes remained slightly dark and tube-like. This type of core−shell heterostructure is termed a MWCNT/GONR nanomaterial. When using the highest microwave power (250 W), a totally flat graphene structure was obtained, as shown in Figure 1d. In their perspectives article, Vázquez and Prato reviewed the mechanism of the carbon nanotube−microwave

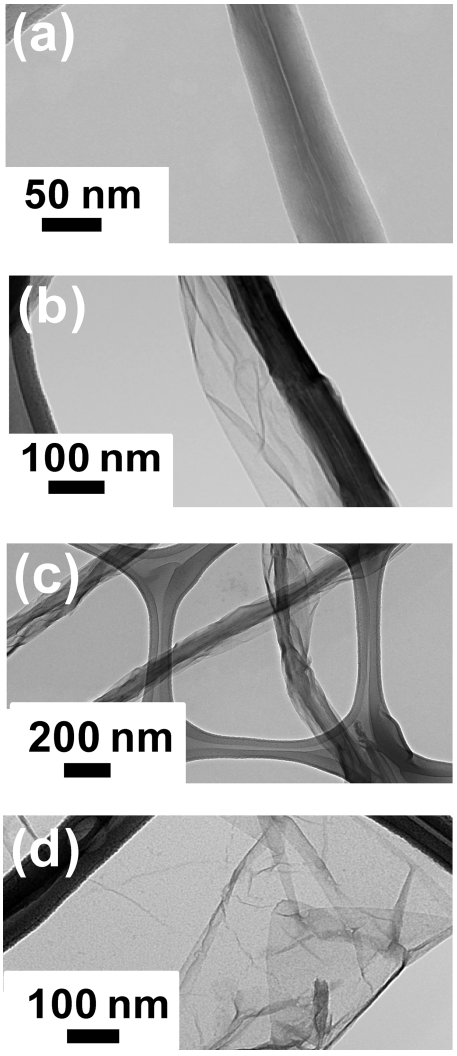

Figure 1. Transmission electron microscopy images of (a) a single as-received multiwalled carbon nanotube and graphene oxide nanoribbons derived from unzipping by treatment with $H_2SO_4 + H_3PO_4$ with dissolved $KMnO_4$ under microwave powers of (b) 150 W, (c) 200 W, and (d) 250 W applied for 4 min.

interaction.[39] A simple model was proposed to explain the microwave-induced heating of CNTs through the transformation of electromagnetic energy into mechanical vibrations. Within this model, CNTs subjected to microwave radiation undergo ultraheating because of a transverse parametric resonance that arises from the polarization of CNTs in the microwave field. In addition to TEM, all samples were also analyzed by Raman spectroscopy. In Figure S1 (Supporting Information), the D band, G band, and 2D band are identified for all samples. With an increase in microwave power, the I_D/I_G ratios of GONRs were found to be higher than those of MWCNTs, indicating a decrease in the size of the sp^2-hybridized carbon domain during the unzipping process. The reduction of GONRs was also performed by annealing in a tube furnace with H_2 flowing for 1 h. Selected samples were characterized using Fourier transform infrared (FTIR) spectroscopy. In Figure S2, the postreduction GNRs are characterized by the almost complete elimination of the COO−H/O−H stretching region (~3600−2800 cm^{-1}, gray region), which implies a decrease in the number of carboxyl and hydroxyl functional groups because of the reduction procedure.

The above-mentioned products were used to modify glassy carbon (GC) electrodes to detect AA, DA, and UA electrochemically using cyclic voltammetry (CV) and differential pulse voltammetry (DPV). Figure 2a−c shows the cyclic voltammograms of various modified GC electrodes produced when sensing 1 mM AA, DA, and UA, respectively. Combined with the results shown in Figure S3 and Table S1, these results indicate that the GONR derived from the reaction with a microwave power of 200 W, GONR(200 W), outperforms all of the other electrode materials in terms of the peak currents in the CV curves. The GONR(200 W) has the core−shell MWCNT/GONR heterostructure mentioned above. For the detection of AA, the peak current of a GONR(200 W)/GC electrode can reach 127.8 μA with a lower peak potential than that of the other materials, indicating better peak separation. For the detection of DA and UA, the peak currents of GONR(200 W) in Figure 2b,c are 455.1 and 475.6 μA, respectively, which are 10 times higher than those of the MWCNTs. It has been found that the open ends of MWCNTs generated by acid treatments can provide higher electrochemical reactivities than those of MWCNTs with closed ends.[76] A considerable body of literature also assumes that the CNT side wall is inert and that edge-plane graphite-like open ends and defect sites are responsible for the observed electron transfer activity.[58] Therefore, it has been suggested that many dangling bonds on the edges of the GONRs may be responsible for the enhanced electrochemical sensing after the unzipping process. On the one hand, GONRs exhibit longer edge-plane structures along the long axis than MWCNTs. On the other hand, GONRs have narrower widths and thus

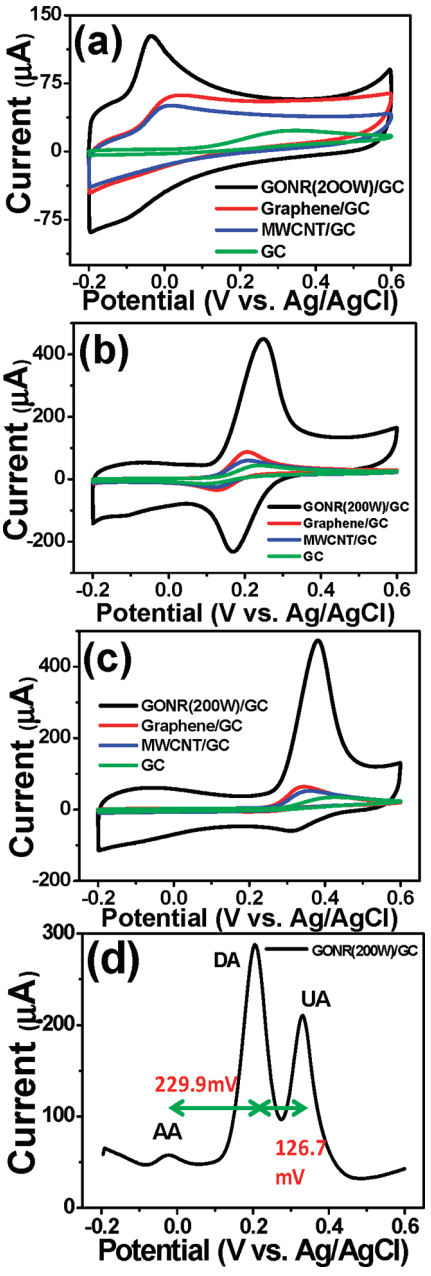

Figure 2. Cyclic voltammograms of GONR(200 W)-, graphene-, and MWCNT-modified GC electrodes and the bare GC electrode in 0.1 M PBS (pH 7.0) containing (a) 1 mM AA, (b) 1 mM DA, and (c) 1 mM UA at a scan rate of 50 mV s^{-1}. (d) Differential pulse voltammetry curve of a GONR(200 W)/GC electrode in a solution containing 0.33 mM AA + 0.033 mM UA + 0.033 mM DA.

more area-normalized edge-plane structures than graphene. It has been demonstrated that the restaking problem of graphene can be solved by adding carbon nanotubes between flat graphene sheets.[77] In the core−shell MWCNT/GONR heterostructure, that is, GONR(200 W), the nonflat cross section of the central MWCNT would also prevent the restaking problem. Therefore, it has been proposed that the central MWCNT core provides a path for rapid electron transport, whereas the outer GONR shell offers many active

sites for fast electrochemical reactions. Furthermore, the electrochemical behavior of a GONR(200 W)/GC electrode in a solution containing a mixture of the three analytes was studied. Figure 2d shows the DPV curve of a GONR(200 W)/GC electrode in a solution of 0.33 mM AA + 0.033 mM DA + 0.033 mM UA. The voltammetric peak separations of AA−DA and DA−UA are 229.9 and 126.7 mV, respectively, which are comparable to those of a graphene/Pt GC electrode.[73] We also used a GONR(200 W)/GC electrode to detect DA with 0.5 mM AA and 0.005 mM UA using differential pulse voltammetry. In Figure S5a, the oxidation current of DA increases with an increase in the DA concentration. When the concentration of DA is greater than 100 μM, the oxidation current increases slowly. In contrast, as shown in Figure S5b, the DA oxidation current is linearly proportional to its concentration in the low concentration range, from 0.5 to 50 μM. Figure S6 shows that there are two different slopes in the plot of current *versus* concentration, and the linear regression equations for the two different regions are also given. In the low-concentration range, the steep slope corresponds to the high sensitivity of the GONR(200 W)/GC electrode for the detection of DA. Compared with the data from the literature presented in Table S2, the dynamic range and detection limit using a GONR-(200 W)/GC electrode without further modification are comparable to those of other nanocarbon-modified GC electrodes found in the literature.

The amperometric responses of the GONR(200 W)-modified GC electrode to AA, DA, and UA are depicted in Figure 3. After adding analyte solutions with different concentrations into a stirred 0.10 M phosphate buffer solution (PBS, pH 7.0) containing 0.1 M KCl, the oxidation currents of specific analytes were monitored at a fixed potential. The corresponding plots of the currents and analyte concentrations are summarized in Figure S4. From the amperometric curve for sensing AA in Figure 3a, the linear relationship between the oxidation current and the AA concentration was obtained for concentrations ranging from 0.1 to 8.5 μM. As indicated in Table S3, the linear regression equation is given by $I_{AA} = 0.1188 + 0.2938C_{AA}$, with a correlation coefficient of $r = 0.9824$ ($N = 3$). The detection limit of AA using a GONR(200 W)/GC electrode was found to be 0.06 μM. Figure 3b shows a typical amperogram of a GONR(200 W)/GC electrode obtained at a potential of +0.2 V for different DA concentrations. The linear relationship between the current and the concentration of DA was obtained for the concentration range of 0.15 to 12.15 μM. The linear regression equation is $I_{DA} = 0.2481 + 0.4694C_{DA}$, with a correlation coefficient of $r = 0.9989$ ($N = 3$). The detection limit for DA was found to be 0.08 μM. Similarly, Figure 3c illustrates the amperogram for UA at a potential of +0.3 V. The linear relationship of UA was determined for UA concentrations ranging from 0.15 to 11.4 μM. The linear

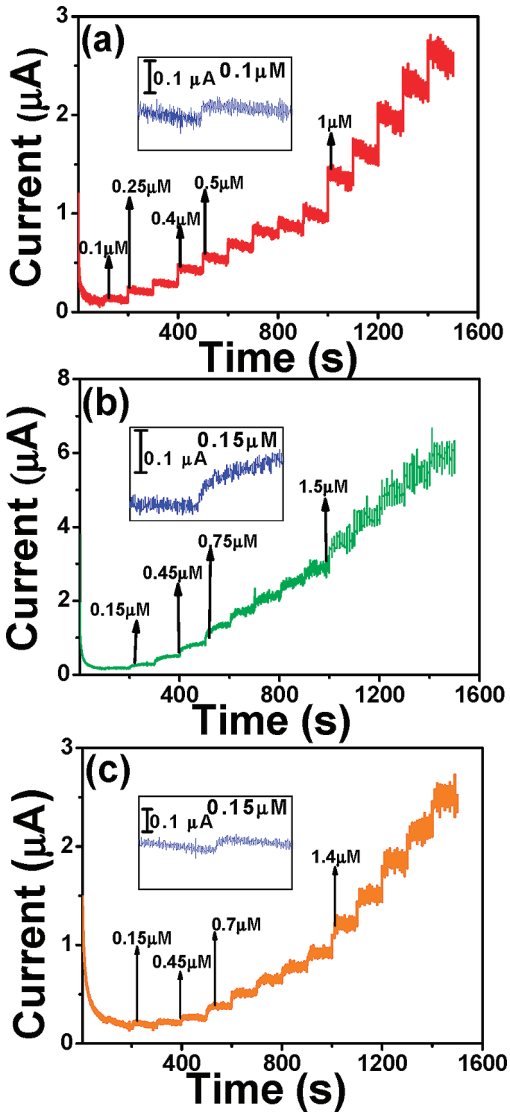

Figure 3. Amperometric responses of a GONR(200 W)-modified GC electrode after the subsequent addition of (a) AA (0.0 V), (b) DA (0.2 V), and (c) UA (0.3 V) in a 0.1 M PBS solution. Inset: corresponding calibration curves of (a) 0.10 μM AA, (b) 0.15 μM DA, and (c) 0.15 μM UA.

regression equation is $I_{UA} = -0.0023 + 0.2154C_{UA}$, with a correlation coefficient of $r = 0.9979$ ($N = 3$). The detection limit of UA was found to be 0.07 μM. The insets in Figure 3 are the calibration curves for 0.10 μM AA, 0.15 μM DA, and 0.15 μM UA. All of the analytical parameters for Figure S4 are summarized in Table S3. In Tables S4 and S5, the data obtained from using a GONR(200 W)/GC electrode for detection of DA, AA, and UA by CV and $i-t$ measurements were compared with those using other electrodes found in the literature.

The electronic structure and morphology of the MWCNT/GONR heterostructure, that is, GONR(200 W) prepared from the unzipping of MWCNT, were studied by X-ray absorption near-edge structure spectroscopy (XANES) using a scanning transmission X-ray microscope (STXM) at the SM beamline of the Canadian Light

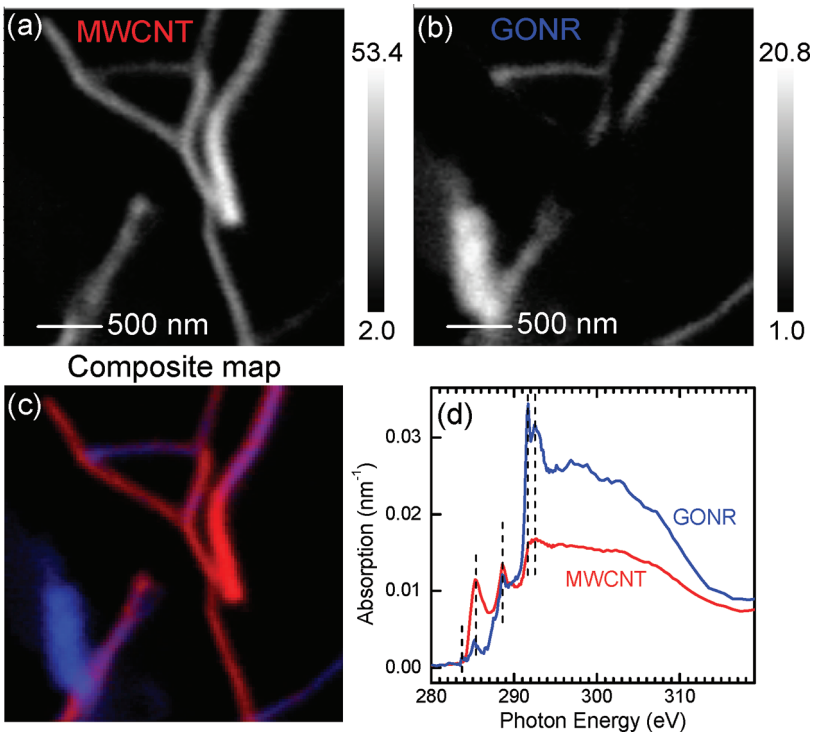

Figure 4. Quantitative chemical mapping of the MWCNT/GONR heterostructure, i.e., GONRs(200 W). (a) MWCNTs, (b) GONRs, and (c) color composite map with MWCNTs (red) and GONRs (blue); the vertical gray scales of (a) and (b) represent sample thickness in nanometers. (d) C K-edge XANES of GONRs and MWCNTs from each pure region in (c) quantitatively scaled to absorbance per nanometer.

Source. In STXM, the monochromatic X-ray beam is focused by a Fresnel zone plate at a 30 nm point on the sample, and the sample is raster-scanned with the synchronized detection of transmitted X-rays to generate image sequences (stacks) over a range of photon energies across the elemental edges of interest.[78] XANES nanospectroscopic data can be obtained from any physical location on the image stacks, from a single pixel to a desired area of the specimen of interest, and chemical mapping can be derived by fitting the X-ray absorption at each pixel of the image stacks to a combination of reference XANES spectra of pure materials. With the reference spectra quantitatively scaled to absorbance per nanometer of thickness, quantitative chemical mapping in terms of sample thickness can be obtained.[79,80] Figure 4a–c presents the quantitative chemical mapping of several individual MWCNT/GONR heterostructures, which clearly show the distribution of STXM-determined material thickness and the core/shell structure in the color composite image. From the chemical mapping, pure regions of both GONR and MWCNT were identified, and the electronic structure of pure GONR was studied by C K-edge XANES and compared to that of pure MWCNT in Figure 4d. The transitions at 285.3 and 291.7 eV are C 1s transitions to C 2p projected π^* and σ^*, respectively. The presence of these features in both GONRs and MWCNTs provides strong evidence for the existence of an sp^2 carbon network. Relative to MWCNTs, the decrease of π^* in GONRs is attributable to the flat nature of GONRs, which is due to the opening of the MWCNTs, and the flat region is not selected by an in-plane polarized X-ray.[81] The peak at 288.5 eV in GONRs and MWCNTs is attributed to oxygen functional groups (most likely carboxylic groups). This peak in both the GONRs and MWCNTs that was studied in this work was much stronger than in naturally prepared CNTs and graphene,[79,81] indicating that the samples were substantially oxidized, which partly accounts for the enhanced catalytic performance. A small peak at 283.7 eV just before π^* was observed in the GONRs, which is a sign of structural defects. This transition was absent in the MWCNTs. More interestingly, even though the structural defects were evident, as indicated by this peak and the carboxylic functional groups in the GONRs, its σ^* transitions (at 291.7 and 292.7 eV) were well resolved; this observation strongly suggests the presence of a well-organized sp^2 carbon network.[81] Thus, it is plausible that these structural defects are predominately located along the edge of the GONRs, while the interior of the GONRs has a sp^2 carbon network close to that of a perfect graphene sheet. Such morphology has significant implications on the outstanding electrochemical performance observed in this study. Furthermore, GONRs present a much higher unoccupied density of states than do MWCNTs; therefore, their relative electrochemical performance should be affected by this property.[81]

CONCLUSIONS

In summary, a unique microwave-assisted unzipping process has been reported for the synthesis of GONRs. The reaction time of this microwave process was very short compared with that reported in the literature.[21−23] The power-dependent GONR structures created from the unzipping of MWCNTs were characterized and used for the detection of AA, DA, and UA. The optimal microwave power and the resulting core−shell MWCNT/GONR heterostructure provide superior oxidation currents for the three analytes compared with those of MWCNTs and graphene. The electronic structure of the MWCNT/GONR heterostructure revealed by STXM and XANES strongly suggests that the high density of unoccupied electronic states above the Fermi level as well as the enriched oxygen-based functionality at the edge of the graphene-like framework could be responsible for its extraordinary electrochemical properties. It is believed that this proposed process can be used for the large-scale and efficient production of GONRs. Additionally, on the basis of the electrochemical measurements, the core−shell MWCNT/GONR heterostructure exhibits a great degree of potential for use as a novel biosensing platform.

METHODS

Chemicals. MWCNTs were used as received from Mitsui & Co. (product name, NCT tube; diameter = 40−90 nm; length = >10 μm). Sulfuric acid (H_2SO_4), phosphoric acid (H_3PO_4), and potassium permanganate ($KMnO_4$) were purchased from J.T.Baker. Nafion (DuPont, 5 wt %) was used to generate the ink. AA, DA, and UA were obtained from Sigma. All solutions were prepared with deionized water with a resistivity of 18 MΩ/cm. Graphene oxide powders were prepared following Staudenmaier's method and reduced to graphene powders by annealing at 1050 °C under an argon atmosphere.[82,83]

Microwave-Assisted Synthesis of GONR. MWCNTs (0.05 g) were suspended in 9:1 H_2SO_4/H_3PO_4 and treated with a microwave reactor (CEM-Discover) with the power set between 150 and 250 W for 2 min. After the addition of $KMnO_4$ (0.25 g) to the solutions,[21,22] the solutions were treated with the same microwave power at 65 °C for 4 min. In 2010, Higginbotham *et al.* reported an improved method for the production of GONRs *via* the unzipping process.[23] This new, optimized method, which introduces a second, weaker acid such as H_3PO_4 into the system, improves the selectivity of the oxidative unzipping, presumably by the *in situ* protection of the vicinal diols formed on the basal plane of graphene during oxidation and thereby prevents their overoxidation and subsequent hole generation. The solutions were filtered through a Millipore membrane (0.1 μm pore size), and the solid products were washed with water several times.

Material Characterization. Transmission electron microscopy (JEOL JEM-1230, 100 kV) was used to characterize sample morphologies. Confocal micro-Raman spectroscopy (Jobin-Yvon LabRAM HR800) was used to analyze the samples at a laser wavelength of 633 nm. Fourier transform infrared (FTIR) spectroscopy was performed using an FTIR (Bruker, Tensor 27) spectrometer.

Preparation of Modified Electrodes. The different powders (6 mg) were mixed with deionized water (3 mL), ethanol (2 mL), and Nafion (60 μL) and then ultrasonically treated to form the inks. Approximately 10 μL of each ink was dropped onto a clean GC electrode and dried at room temperature to form the modified GC electrodes.

Electrochemical Measurements. Electrochemical experiments were performed with a CHI 7031D electrochemical workstation (CHI, USA). A standard three-electrode cell was used for the electrochemical experiments. A 5 mm diameter GC was used as the working electrode (working area of 0.19625 cm^2). A silver/silver chloride (Ag/AgCl) electrode and a platinum (Pt) electrode were used as the reference and the counter electrodes, respectively. All potentials in this study are reported with respect to the Ag/AgCl electrode. The measurements were performed in a phosphate buffer solution (PBS) with 0.1 M KCl at a pH of 7.0 at room temperature.

Scanning Transmission X-ray Microscope Measurements and X-ray Absorption Near-Edge Structure Spectroscopy. A powder sample was dispersed in alcohol before deposition on a Si_3N_4 window for STXM measurement. The STXM measurement was conducted using the STXM at the SM beamline of the Canadian Light Source (CLS), a 2.9 GeV third-generation synchrotron facility. A 25 nm outermost-zone zone plate (CXRO, Berkeley Lab) was used, which provides a spatial resolution of 30 nm. A circularly polarized soft X-ray beam generated from the SM elliptically polarized undulator (EPU) was used to average out the in-plane polarization dependence of the sample. The C K-edge image sequence (stack) covered an energy range of 280−320 eV, with energy steps as fine as 0.1 eV around the XANES peaks, and an energy range of 0.4−1.0 eV in the pre-edge and continuum. The image pixel size was 25 nm, with a 1 ms dwell time per pixel. STXM data were analyzed with aXis2000 (available free at http://unicorn.mcmaster.ca/aXis2000.html). XANES reference spectra of GONRs and MWCNTs were extracted from each pure region in the C K-edge image stack, and they were then quantitatively scaled to the elemental X-ray absorption profiles of graphite (density = 2.16 g/cm^3, 1 nm thick) and CNTs (density = 1.8 g/cm^3, 1 nm thick) in the pre-edge and the post-edge, respectively. Quantitative chemical mapping was performed by fitting the C K-edge image stack to the reference spectra of GONRs and MWCNTs. Finally, a color composite map was created by combining individual component maps with the image intensity rescaled for better visualization.

Acknowledgment. The authors gratefully acknowledge the financial support from the National Science Council and Chang Gung University. Research at the CLS was supported by NSERC, NRC, CIHR of Canada, and the University of Saskatchewan. Research at UWO was supported by NSERC, CFI, CRC, and OIT.

Supporting Information Available: Raman spectra, FTIR spectra, and the analytical results of amperometric measurements. This material is available free of charge *via* the Internet at http://pubs.acs.org.

REFERENCES AND NOTES

1. Kroto, H. W.; Heath, J. R.; O'Brien, S. C.; Curl, R. F.; Smalley, R. E. C_{60}: Buckminsterfullerene. *Nature* **1985**, *318*, 162.
2. Iijima, S. Helical Microtubules of Graphitic Carbon. *Nature* **1991**, *354*, 56.
3. Ebbesen, T. W.; Ajayan, P. M. Large-Scale Synthesis of Carbon Nanotubes. *Nature* **1992**, *358*, 220–222.
4. Chen, L. C.; Wen, C. Y.; Liang, C. H.; Hong, W. K.; Chen, K. J.; Cheng, H. C.; Shen, C. S.; Wu, C. T.; Chen, K. H. Controlling Steps during Early Stages of the Aligned Growth of Carbon Nanotubes Using Microwave Plasma Enhanced Chemical Vapor Deposition. *Adv. Funct. Mater.* **2002**, *12*, 687–692.
5. Sun, C. L.; Chen, L. C.; Su, M. C.; Hong, L. S.; Chyan, O.; Hsu, C. Y.; Chen, K. H.; Chang, T. F.; Chang, L. Ultrafine Platinum Nanoparticles Uniformly Dispersed on Arrayed CN_x Nanotubes with High Electrochemical Activity. *Chem. Mater.* **2005**, *17*, 3749–3753.

6. Sun, C. L.; Wang, H. W.; Hayashi, M.; Chen, L. C.; Chen, K. H. Atomic-Scale Deformation in N-Doped Carbon Nanotubes. *J. Am. Chem. Soc.* **2006**, *128*, 8368–8369.
7. Gheith, M. K.; Pappas, T. C.; Liopo, A. V.; Sinani, V. A.; Shim, B. S.; Motamedi, M.; Wicksted, J. P.; Kotov, N. A. Stimulation of Neural Cells by Lateral Layer-by-Layer Films of Single-Walled Currents in Conductive Carbon Nanotubes. *Adv. Mater.* **2006**, *18*, 2975–2979.
8. Shim, B. S.; Zhu, J.; Jan, E.; Critchley, K.; Ho, S.; Podsiadlo, P.; Sun, K.; Kotov, N. A. Multiparameter Structural Optimization of Single-Walled Carbon Nanotube Composites: Toward Record Strength, Stiffness, and Toughness. *ACS Nano* **2009**, *3*, 1711–1722.
9. Shim, B. S.; Zhu, J.; Jan, E.; Critchley, K.; Kotov, N. A. Transparent Conductors from Layer-by-Layer Assembled SWNT Films: Importance of Mechanical Properties and a New Figure of Merit. *ACS Nano* **2010**, *4*, 3725–3734.
10. Novoselov, K. S.; Geim, A. K.; Morozov, S. V.; Jiang, D.; Zhang, Y.; Dubonos, S. V.; Grigorieva, I. V.; Firsov, A. A. Electric Field Effect in Atomically Thin Carbon Films. *Science* **2004**, *306*, 666–668.
11. Novoselov, K. S.; Geim, A. K.; Morozov, S. V.; Jiang, D.; Katsnelson, M. I.; Grigorieva, I. V.; Dubonos, S. V.; Firsov, A. A. Two-Dimensional Gas of Massless Dirac Fermions in Graphene. *Nature* **2005**, *438*, 197–200.
12. Geim, A. K.; Novoselov, K. S. The Rise of Graphene. *Nat. Mater.* **2007**, *6*, 183.
13. Dimiev, A.; Kosynkin, D. V.; Sinitskii, A.; Slesarev, A.; Sun, Z.; Tour, J. M. Layer-by-Layer Removal of Graphene for Device Patterning. *Science* **2011**, *331*, 1168–1172.
14. Nakada, K.; Fujita, M.; Dresselhaus, G.; Dresselhaus, M. S. Edge State in Graphene Ribbons: Nanometer Size Effect and Edge Shape Dependence. *Phys. Rev. B* **1996**, *54*, 17954–17961.
15. Tapaszto, L.; Dobrik, G.; Lambin, P.; Biro, L. P. Tailoring the Atomic Structure of Graphene Nanoribbons by Scanning Tunnelling Microscope Lithography. *Nat. Nanotechnol.* **2008**, *3*, 397–401.
16. Campos-Delgado, J.; Romo-Herrera, J. M.; Jia, X.; Cullen, D. A.; Muramatsu, H.; Kim, Y. A.; Hayashi, T.; Ren, Z.; Smith, D. J.; Okuno, Y.; *et al.* Bulk Production of a New Form of sp^2 Carbon: Crystalline Graphene Nanoribbons. *Nano Lett.* **2008**, *8*, 2773–2778.
17. Son, Y. W.; Cohen, M. L.; Louie, S. G. Energy Gaps in Graphene Nanoribbons. *Phys. Rev. Lett.* **2006**, *97*, 216803.
18. Li, X.; Wang, X.; Zhang, L.; Lee, S.; Dai, H. Chemically Derived, Ultrasmooth Graphene Nanoribbon Semiconductors. *Science* **2008**, *319*, 1229.
19. Terrones, M. Unzipped Nanotubes. *Nature* **2009**, *458*, 845–846.
20. Terrones, M. Sharpening the Chemical Scissors to Unzip Carbon Nanotubes: Crystalline Graphene Nanoribbons. *ACS Nano* **2010**, *4*, 1775–1781.
21. Kosynkin, D. V.; Higginbotham, A. L.; Sinitskii, A.; Lomeda, J. R.; Dimiev, A.; Price1, B. K.; Tour, J. M. Longitudinal Unzipping of Carbon Nanotubes To Form Graphene Nanoribbons. *Nature* **2009**, *458*, 16.
22. Zhang, Z.; Sun, Z.; Yao, J.; Kosynkin, D. V.; Tour, J. M. Transforming Carbon Nanotube Devices into Nanoribbon Devices. *J. Am. Chem. Soc.* **2009**, *131*, 13460.
23. Higginbotham, A. L.; Kosynkin, D. V.; Sinitskii, A.; Sun, Z.; Tour, J. M. Lower-Defect Graphene Oxide Nanoribbons from Multiwalled Carbon Nanotubes. *ACS Nano* **2010**, *4*, 2059–2069.
24. Jiao, L.; Zhang, L.; Wang, X.; Diankov, G.; Dai, H. Narrow Graphene Nanoribbons from Carbon Nanotube. *Nature* **2008**, *458*, 877–880.
25. Abraham, G.; Cano, M.; Fernando, J.; Rodríguez, M.; Jessica, C. D.; Claudia, G.; Espinosa, G.; Ferdinando, T. L.; Daniel, R. G.; Cullen, D. A.; *et al.* Ex-MWNTs: Graphene Sheets and Ribbons Produced by Lithium Intercalation and Exfoliation of Carbon Nanotubes. *Nano Lett.* **2009**, *9*, 1527.
26. Ci, L.; Xu, Z.; Wang, L.; Gao, W.; Ding, F.; Kelly, K. F.; Yakobson, B. I.; Ajayan, P. M. Controlled Nanocutting of Graphene. *Nano Res.* **2008**, *1*, 116.
27. Elías, A. L.; Botello-Méndez, A. R.; Meneses-Rodríguez, D.; González, V. J.; Ramírez-González, D.; Ci, L.; Muñoz-Sandoval, E.; Ajayan, P. M.; Terrones, H.; Terrones, M. Longitudinal Cutting of Pure and Doped Carbon Nanotubes To Form Graphitic Nanoribbons Using Metal Clusters as Nanoscalpels. *Nano Lett.* **2010**, *10*, 366–372.
28. Kim, K.; Sussman, A.; Zettl, A. Graphene Nanoribbons Obtained by Electrically Unwrapping Carbon Nanotubes. *ACS Nano* **2010**, *4*, 1362–1366.
29. Wu, Z. S.; Ren, W.; Gao, L.; Liu, B.; Zhao, J.; Cheng, H. M. Efficient Synthesis of Graphene Nanoribbons Sonochemically Cut from Graphene Sheets. *Nano. Res.* **2010**, *3*, 16–22.
30. Shinde, D. B.; Debgupta, J.; Kushwaha, A.; Aslam, M.; Pillai, V. K. Electrochemical Unzipping of Multi-walled Carbon Nanotubes for Facile Synthesis of High-Quality Graphene Nanoribbons. *J. Am. Chem. Soc.* **2011**, *133*, 4168–4171.
31. Kingston, H. M.; Haswell, S. J. *Microwave-Enhanced Chemistry: Fundamentals, Sample Preparation, and Applications*; ACS Publication: Washington DC, 1997.
32. Gerbec, J. A.; Magana, D.; Washington, A.; Strouse, G. F. Microwave-Enhanced Reaction Rates for Nanoparticle Synthesis. *J. Am. Chem. Soc.* **2005**, *127*, 15791–15800.
33. Artman, D. D.; Grubbs, A. W.; Williams, R. M. Concise, Asymmetric, Stereocontrolled Total Synthesis of Stephacidins A, B and Notoamide B. *J. Am. Chem. Soc.* **2007**, *129*, 6336–6342.
34. Huang, H.; Sithambaram, S.; Chen, C. H.; Kithongo, C. K.; Xu, L.; Iyer, A.; Garces, H. F.; Suib, S. L. Microwave-Assisted Hydrothermal Synthesis of Cryptomelane-Type Octahedral Molecular Sieves (OMS-2) and Their Catalytic Studies. *Chem. Mater.* **2010**, *22*, 3664–3669.
35. Chang, K. H.; Lee, Y. F.; Hu, C. C.; Chang, C. I.; Liu, C. L.; Yang, Y. L. A Unique Strategy for Preparing Single-Phase Unitary/Binary Oxides−Graphene Composites. *Chem. Commun.* **2010**, *46*, 7957–7959.
36. Zhu, Y.; Murali, S.; Stoller, M. D.; Ganesh, K. J.; Cai, W.; Ferreira, P. J.; Pirkle, A.; Wallace, R. M.; Cychosz, K. A.; Thommes, M.; *et al.* Carbon-Based Supercapacitors Produced by Activation of Graphene. *Science* **2011**, *332*, 1537–1541.
37. Imholt, T. J.; Dyke, C. A.; Hasslacher, B.; Perez, J. M.; Price, D. W.; Roberts, J. A.; Scott, J. B.; Wadhawan, A.; Ye, Z.; Tour, J. M. Nanotubes in Microwave Fields: Light Emission, Intense Heat, Outgassing, and Reconstruction. *Chem. Mater.* **2003**, *15*, 3969–3970.
38. Paton, K. R.; Windle, A. H. Efficient Microwave Energy Absorption by Carbon Nanotubes. *Carbon* **2008**, *46*, 1935–1941.
39. Vázquez, E.; Prato, M. Carbon Nanotubes and Microwaves: Interactions, Responses, and Applications. *ACS Nano* **2009**, *3*, 3819–3824.
40. Murugan, A. V.; Muraliganth, T.; Manthiram, A. Rapid, Facile Microwave-Solvothermal Synthesis of Graphene Nanosheets and Their Polyaniline Nanocomposites for Energy Strorage. *Chem. Mater.* **2009**, *21*, 5004–5006.
41. Harutyunyan, A. R.; Pradhan, B. K.; Chang, J.; Chen, G.; Eklund, P. C. Purification of Single-Wall Carbon Nanotubes by Selective Microwave Heating of Catalyst Particles. *J. Phys. Chem. B* **2002**, *106*, 8671–8675.
42. Della Negra, F.; Meneghetti, M.; Menna, E. Microwave-Assisted Synthesis of a Soluble Single Wall Carbon Nanotube Derivative. *Fullerenes, Nanotubes, Carbon Nanostruct.* **2003**, *11*, 25.
43. Raghuveer, M. S.; Agrawal, S.; Bishop, N.; Ramanath, G. Microwave-Assisted Single-Step Functionalization and *In Situ* Derivatization of Carbon Nanotubes with Gold Nanoparticles. *Chem. Mater.* **2006**, *18*, 1390–1393.
44. Lin, K. M.; Changa, K. H.; Hua, C. C.; Li, Y. Y. Mesoporous RuO_2 for the Next Generation Supercapacitors with an Ultrahigh Power Density. *Electrochim. Acta* **2009**, *54*, 4574–4581.
45. Carlsson, A.; Lindqvist, M.; Magnusson, T. 3,4-Dihydroxyphenylalanine and 5-Hydroxytryptophan as Reserpine Antagonists. *Nature* **1957**, *180*, 1200.
46. Savitt, J. M.; Dawson, V. L.; Dawson, T. M. Diagnosis and Treatment of Parkinson Disease: Molecules to Medicine. *J. Clin. Invest.* **2006**, *116*, 1744–1754.

47. Adams, R. N. Probing Brain Chemistry with Electroanalytical. *Anal. Chem.* **1976**, *48*, 1126–1137.
48. Lane, R. F.; Hubbard, A. T.; Blaha, C. D. 243-Brain Dopaminergic Neurons: *In Vivo* Electrochemical Information Concerning Storage, Metabolism and Release Processes. *Bioelectrochem. Bioenerg.* **1978**, *5*, 504–525.
49. Gonon, F. G.; Fombarlet, C. M.; Buda, M. J.; Pujol, J. F. Electrochemical Treatment of Pyrolytic Carbon Fiber Electrodes. *Anal. Chem.* **1981**, *53*, 1386–1389.
50. Falat, L.; Cheng, H. Y. Voltammetric Differentiation of Ascorbic Acid and Dopamine at an Electrochemically Treated Graphite/Epoxy Electrode. *Anal. Chem.* **1982**, *54*, 2108–2111.
51. Chen, M.; Li, H. Separation of Anodic Peaks of Ascorbic Acid and Dopamine at 4-Hydroxy-2-mercapto-6-methylpyrimidine Modified Gold Electrode. *Electroanalysis* **1998**, *10*, 477–479.
52. Aguilar, R.; Dávila, M. M.; Elizalde, M. P.; Mattusch, J.; Wennrich, R. Capability of a Carbon–Polyvinylchloride Composite Electrode for the Detection of Dopamine, Ascorbic Acid and Uric Acid. *Electrochim. Acta* **2004**, *49*, 851–859.
53. Ensafi, A. A.; Taei, M.; Khayamian, T.; Arabzadeh, A. Highly Selective Determination of Ascorbic Acid, Dopamine, and Uric Acid by Differential Pulse Voltammetry Using Poly(sulfonazo III) Modified Glassy Carbon Electrode. *Sens. Actuators, B* **2010**, *147*, 213–221.
54. Ensafi, A. A.; Rezaei, B.; Zare, S. Z. M.; Taei, M. Simultaneous Determination of Ascorbic Acid, Epinephrine, and Uric Acid by Differential Pulse Voltammetry Using Poly(3,3′-bis[*N*,*N*-bis(carboxymethyl)aminomethyl]-*o*-cresolsulfonephthalein) Modified Glassy Carbon Electrode. *Sens. Actuators, B* **2010**, *150*, 321–329.
55. Wang, J.; Musameh, M. Carbon Nanotube/Teflon Composite Electrochemical Sensors and Biosensors. *Anal. Chem.* **2003**, *75*, 2075–2079.
56. Kim, S. N.; Rusling, J. F.; Papadimitrakopoulos, F. Carbon Nanotubes for Electronic and Electrochemical Detection of Biomolecules. *Adv. Mater.* **2007**, *19*, 3214–3228.
57. McCreery, R. L. Advanced Carbon Electrode Materials for Molecular Electrochemistry. *Chem. Rev.* **2008**, *108*, 2646–2687.
58. Dumitrescu, I.; Unwin, P. R.; Macpherson, J. V. Electrochemistry at Carbon Nanotubes: Perspective and Issues. *Chem. Commun.* **2009**, *45*, 6865–7052.
59. Zhang, Y.; Cai, Y.; Su, S. Determination of Dopamine in the Presence of Ascorbic Acid by Poly(styrene sulfonic acid) Sodium Salt/Single-Wall Carbon Nanotube Film Modified Glassy Carbon Electrode. *Anal. Biochem.* **2006**, *350*, 285–291.
60. Wang, H. S.; Li, T. H.; Jia, W. L.; Xu, H. Y. Highly Selective and Sensitive Determination of Dopamine Using a Nafion/Carbon Nanotubes Coated Poly(3-methylthiophene) Modified Electrode. *Biosens. Bioelectron.* **2006**, *22*, 664–669.
61. Yogeswaran, U.; Chen, S. M. Separation and Concentration Effect of *f*-MWCNTs on Electrocatalytic Responses of Ascorbic Acid, Dopamine and Uric Acid at *f*-MWCNTs Incorporated with Poly (neutral red) Composite Films. *Electrochim. Acta* **2007**, *52*, 5985–5996.
62. Kumar, S. A.; Wang, S. F.; Yang, T. C. K.; Yeh, C. T. Acid Yellow 9 as a Dispersing Agent for Carbon Nanotubes: Preparation of Redox Polymer–Carbon Nanotube Composite Film and Its Sensing Application towards Ascorbic Acid and Dopamine. *Biosens. Bioelectron.* **2010**, *25*, 2592–2597.
63. Lin, K. C.; Tsai, T. H.; Chen, S. M. Performing Enzyme-Free H_2O_2 Biosensor and Simultaneous Determination for AA, DA, and UA by MWCNT–PEDOT Film. *Biosens. Bioelectron.* **2010**, *26*, 608–614.
64. Ambrosi, A.; Sasaki, T.; Pumera, M. Platelet Graphite Nanofibers for Electrochemical Sensing and Biosensing: The Influence of Graphene Sheet Orientation. *Chem. Asian J.* **2010**, *5*, 266–271.
65. Tang, L.; Wang, Y.; Li, Y.; Feng, H.; Lu, J.; Li, J. Preparation, Structure, and Electrochemical Properties of Reduced Graphene Sheet Films. *Adv. Funct. Mater.* **2009**, *19*, 2782–2789.
66. Chen, D.; Tang, L.; Li, J. Graphene-Based Materials in Electrochemistry. *Chem. Soc. Rev.* **2010**, *39*, 3157–3180.
67. Pumera, M. Graphene-Based Nanomaterials and Their Electrochemistry. *Chem. Soc. Rev.* **2010**, *39*, 4146–4157.
68. Shang, N. G.; Papakonstantinou, P.; McMullan, M.; Chu, M.; Stamboulis, A.; Potenza, A.; Dhesi, S. S.; Marchetto, H. Catalyst-Free Efficient Growth, Orientation and Biosensing Properties of Multilayer Graphene Nanoflake Films with Sharp Edge Planes. *Adv. Funct. Mater.* **2008**, *18*, 3506–3514.
69. Zhou, M.; Zhai, Y.; Dong, S. Electrochemical Sensing and Biosensing Platform Based on Chemically Reduced Graphene Oxide. *Anal. Chem.* **2009**, *81*, 5603–5613.
70. Wang, Y.; Li, Y.; Tang, L.; Lu, J.; Li, J. Application of Graphene-Modified Electrode for Selective Detection of Dopamine. *Electrochem. Commun.* **2009**, *11*, 889–892.
71. Lim, C. X.; Hoh, H. Y.; Ang, P. K.; Loh, K. P. Direct Voltammetric Detection of DNA and pH Sensing on Epitaxial Graphene: An Insight into the Role of Oxygenated Defects. *Anal. Chem.* **2010**, *82*, 7387–7393.
72. Kim, Y. R.; Bong, S.; Kang, Y. J.; Yang, Y.; Mahajan, R. K.; Kim, J. S.; Kim, H. Electrochemical Detection of Dopamine in the Presence of Ascorbic Acid Using Graphene Modified Electrodes. *Biosens. Bioelectron.* **2010**, *25*, 2366–2369.
73. Sun, C. L.; Lee, H. H.; Yang, J. M.; Wu, C. C. The Simultaneous Electrochemical Detection of Ascorbic Acid, Dopamine, and Uric Acid Using Graphene/Size-Selected Pt Nanocomposites. *Biosens. Bioelectron.* **2011**, *26*, 3450–3455.
74. Bhardwaj, T.; Antic, A.; Pavan, B.; Barone, V.; Fahlman, B. D. Enhanced Electrochemical Lithium Storage by Graphene Nanoribbons. *J. Am. Chem. Soc.* **2010**, *132*, 12556–12558.
75. Lima, M. D.; Fang, S.; Lepró, X.; Lewis, C.; Ovalle-Robles, R.; Carretero-González, J.; Castillo-Martínez, E.; Kozlov, M. E.; Oh, J.; Rawat, N.; *et al.* Biscrolling Nanotube Sheets and Functional Guests into Yarns. *Science* **2011**, *331*, 51–55.
76. Fang, W. C.; Huang, J. H.; Chen, L. C.; Su, Y. O.; Chen, K. H.; Sun, C. L. Carbon Nanotubes Grown Directly on Ti Electrodes and Enhancement of Their Electrochemical Properties by Nitric Acid Treatment. *Electrochem. Solid-State Lett.* **2006**, *9*, 5–8.
77. Yang, S. Y.; Chang, K. H.; Lee, Y. F.; Ma, C. C. M.; Hu, C. C. Constructing a Hierarchical Graphene–Carbon Nanotube Architecture for Enhancing Exposure of Graphene and Electrochemical Activity of Pt Nanoclusters. *Electrochem. Commun.* **2010**, *12*, 1206–1209.
78. Jacobsen, C.; Wirick, S.; Flynn, G.; Zimba, C. Soft X-ray Spectroscopy from Image Sequences with Sub-100nm Spatial Resolution. *J. Microsc.* **2000**, *197*, 173–184.
79. Zhou, J.; Wang, J.; Fang, H.; Wu, C.; Cutler, J. N.; Sham, T. K. Nanoscale Chemical Imaging and Spectroscopy of Individual RuO_2 Coated Carbon Nanotubes. *Chem. Commun.* **2010**, *46*, 2778–2780.
80. Zhou, J.; Wang, J.; Liu, H.; Banis, M. N.; Sun, X.; Sham, T. K. Imaging Nitrogen in Individual Carbon Nanotubes. *J. Phys. Chem. Lett.* **2010**, *1*, 1709–1713.
81. Zhou, J. G.; Wang, J.; Sun, C. L.; Maley, J. M.; Sammynaiken, R.; Sham, T. K.; Pong, W. F.Nano-scale Chemical Imaging of a Single Sheet of Reduced Graphene Oxide. *J. Mater. Chem.* **2011**, DOI: 10.1039/C1JM11071C.
82. Staudenmaier, L. Verfahren zur Darstellung der Graphitsäure. *Ber. Dtsch. Chem. Ges.* **1898**, *31*, 1481–1487.
83. McAllister, M. J.; Li, J. L.; Adamson, D. H.; Schniepp, H. C.; Abdala, A. A.; Liu, J.; Herrera-Alonso, M.; Milius, D. L.; Car, R.; Prud'homme, R. K.; *et al.* Single Sheet Functionalized Graphene by Oxidation and Thermal Expansion of Graphite. *Chem. Mater.* **2007**, *19*, 4396–4404.